Journal of the Optical Society of Korea, Vol. 10, No. 3, September 2006, pp. 99-104

Nanoparticle Contrast in Magneto-Motive Optical Doppler Tomography

Jee-Hyun Kim*

Beckman Laser Institute and Medical Clinic, University of California, 1002 Health Sciences Road East, Irvine, CA 92612

Jung-Hwan Oh

Biomedical Engineering Department, University of Texas, Austin, TX 78712

(Received July 11, 2006 : revised September 27, 2006)

We introduce a novel contrast mechanism for imaging superparamagnetic iron oxide (SPIO) nanoparticles (average diameter ~ 100 nm) using magneto-motive optical Doppler tomography (MM-ODT), which combines an externally applied temporally oscillating high-strength magnetic field with ODT to detect the nanoparticles flowing through a glass capillary tube. A solenoid cone-shaped ferrite core extensively increased the magnetic field strength (B_{max}=1 T, $\Delta|B|^2 = 220$ T^2/m) at the tip of the core and also focused the magnetic force on targeted samples. Nanoparticle contrast was demonstrated in a capillary tube filled with the SPIO solution by imaging the Doppler frequency shift which was observed independent of the flow rate and direction. Results suggest that MM-ODT may be a promising technique to enhance SPIO nanoparticle contrast for imaging fluid flow.

OCIS codes : 030.1640, 110.0110, 170.0170, 170.1650

I. INTRODUCTION

Optical coherence tomography (OCT) uses the short temporal coherence properties of broadband light to extract structural information from heterogeneous samples such as biologic tissue. During the past decade, numerous advancements in OCT have been reported including cellular-level resolution [1] and real-time imaging speed [2]. Conventional OCT imaging primarily utilizes a single backscattering feature to display intensity images. Functional OCT techniques process the backscattered light to provide additional information on birefringence [3-6], and flow properties [7].

Since the ability to characterize fluid flow velocity using OCT was first demonstrated by Wang et al [8], several phase resolved [9], real-time [10,11] optical Doppler tomography (ODT) approaches have been reported. In ODT, the Doppler frequency shift is proportional to the angle between the probe beam and the scatterer's flow direction. When the two directions are perpendicular, the Doppler shift is zero. Because a *priori* knowledge of the Doppler angle is usually not available, and conventional intensity OCT imaging provides a low contrast image of microvasculature structure, detecting small diameter vessels with slow blood flow rates is difficult. However, the Doppler angle can be estimated [12] by combining the Doppler shift and Doppler bandwidth measurements. The ability to locate precisely the microvasculature is important for diagnostics and treatments requiring characterization of blood flow. Recently, several efforts to introduce novel molecular contrast enhancement have been reported including protein microspheres incorporating nanoparticles into their shells [13], plasmon-resonant gold nanoshells [14], and use of magnetically susceptible micrometer sized particles with an externally applied magnetic field [15]. The latter, which produces a speckle change on magnetic particles has been termed magneto-motive OCT (MM-OCT) [15] and was first demonstrated in a living *Xenopus laevis* tadpole [16].

The use of superparamagnetic iron oxides (SPIOs) nanoparticles as contrast agents for magnetic resonance (MR) imaging of bowel, liver, spleen, lymph nodes, bone marrow, perfusion, and angiography [17] has been extensively studied since the early 1990s [18,19]. Superparamagnetic iron oxides are basically nanometer-sized iron oxide particles which easily interact with a magnetic

field because of the high magnetic volume susceptibility ($\chi \approx 1$). A SPIO with $\chi \approx 1$ suspended in solution and placed in a magnetic field gradient experiences forces and torques that tend to position and align it with respect to the field's direction. Magnetic energy, U, of a SPIO nanoparticle in an external magnetic field is given by,

$$U = -\frac{1}{2}\mathbf{m}\mathbf{B} = -\frac{\Delta\chi V}{2u_0}|\mathbf{B}|^2 \quad (1)$$

where $\mathbf{m}$ is the magnetic moment, $\mathbf{B}$ is the magnetic flux density, V is the particle volume, μ_0 is the permeability of free space, and $\Delta\chi$ is the difference between susceptibility of the nanoparticle and surrounding solution. Magnetic force acting on SPIO nanoparticles becomes:

$$\mathbf{F} = -\nabla U = \nabla\left(\frac{\Delta\chi V}{2u_0}|\mathbf{B}|^2\right) = \Delta\chi V \nabla\left(\frac{|\mathbf{B}|^2}{2u_0}\right) \quad (2)$$

In our experiments we apply a sinusoidal magnetic flux density that is directed principally along the z-direction. Hence, we write $\vec{B}(x, y, z; t) = \sin(2\pi f_m t)\mathrm{B}_z(z)\hat{k}$ and the magnetic force $\mathbf{F_m}$ acting on nanoparticles,

$$\frac{\mathrm{F_m} = \chi_s V_s}{2\mu_0}[1 - \cos(4\pi f_m t)]\mathrm{B}_z(z)\frac{\partial \mathrm{B}_z}{\partial z} \quad (3)$$

where f_m is the modulation frequency of the applied sinusoidal magnetic field.

In addition to the magnetic force, the SPIO nanoparticle experiences a pressure gradient, body, and drag forces which combine to give a dynamic displacement $[z(t)]$ that can be included in the analytic OCT fringe expression, I_f,

$$I_f \propto 2\sqrt{I_R I_S}\exp\left[i\left(2\pi f_0 t + \frac{4\pi n \cdot z(t)}{\lambda_0}\right)\right], \quad (4)$$

where I_R and I_S are the back scattered intensities from reference and sample arms, respectively, f_0 is the fringe carrier frequency, n is the medium refractive index, $z(t)$ is the dynamic nanoparticle displacement, and λ_0 is the light source center wavelength.

Herein we present a novel extension of the magnetomotive approach by modulating phase to improve the magnetic nanoparticle contrast. The contrast of ODT images can be enhanced by activating the nanoparticles with an externally applied high-strength magnetic field gradient. We describe the MM-ODT experimental setup containing an oscillating magnetic field generator, and present M-mode images of the Doppler shift of flowing SPIO nanoparticles under the influence of an externally applied magnetic field gradient.

II. METHOD AND EXPERIMENTAL SETUP

A schematic of the MM-ODT apparatus is shown in Fig. 1. The ODT light source consisted of a super luminescent diode (B&W TEK, DE) centered at 1.3 μm with a bandwidth of 90 nm. Light was coupled into a single-mode optical-fiber-based interferometer that provided 1 mW of optical power at the sample. A rapid-scanning optical delay (RSOD) line was used in the reference arm and aligned such that no phase modulation was generated when the group phase delay was

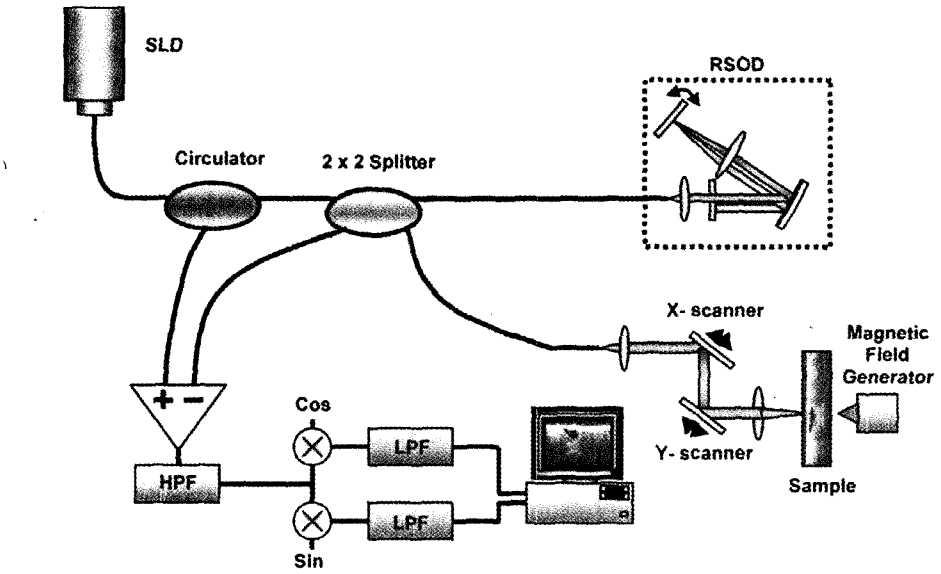

FIG. 1. Schematic diagram of the MM-ODT system. SLD: Super-luminescent diode, HPF: high pass filter, LPF: low pass filter.

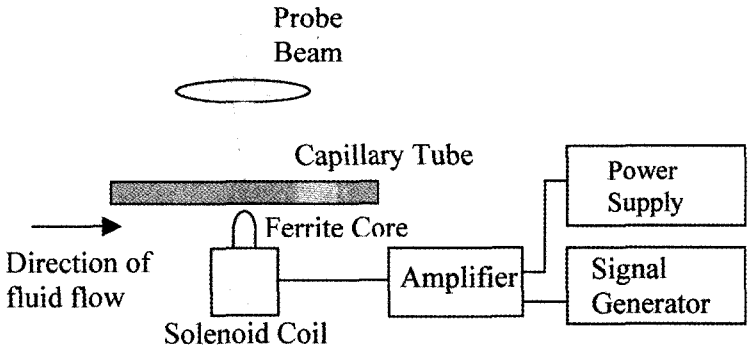

FIG. 2. Schematic diagram of the probe beam, flow sample and solenoid coil.

scanned at 4 kHz. Phase modulation was generated using an electro-optic waveguide phase modulator that produced a single carrier frequency (1 MHz). To reduce light source noise from the OCT interference signal, a dual-balanced photodetector was used. A hardware in-phase and quadrature demodulator with high/bandpass filters was constructed to improve imaging speed. Doppler information was calculated with the Kasai autocorrelation velocity estimator. Labview software (National Instruments, Austin, TX) was used to implement the MM-ODT system with a dual processor based multitasking scheme. The maximum frame rate of the system was 16 frames per second for a 400×512 pixel sized image. In the sample arm, a collimated beam was redirected to the sample by two galvanometers that permited three-dimensional scanning. The probe beam was focused by an objective lens, which yielded a 10 μm diameter spot at the focal point. A 750 μm inner diameter glass capillary tube was placed perpendicularly to the probing beam. Fluids used for flow studies were injected through the tube at a constant flow rate controlled by a dual-syringe pump (Harvard Apparatus 11 Plus, Holliston, MA) with ±0.5% flow rate accuracy.

A solenoid coil (manufacturer: Ledex, part number: 4EF) with a cone-shaped ferrite core at the center (Fig. 2) and driven by a current amplifier supplying up to 960 W, was placed underneath the sample during MM-ODT imaging. The combination of the core and solenoid, using high power operation, dramatically increased the magnetic field strength (B_{max}=1 T and $\Delta|B|^2 = 220\ T^2/m$) at the tip of the core and also focused the magnetic force on the targeted samples. The magnetic force applied to the capillary tube was varied by the sinusoidal current to induce SPIO nanoparticle movement.

Nanoparticle solutions were prepared to observe phase-modulated nanoparticles in a flow channel. Feridex I.V. SPIO nanoparticles nominally 100 nm in size (Advanced Magnetics, Inc.) were used in all experiments. The prepared nanoparticle solution consisted of 50 mL 5% dextrose solution and 1 mL pure Feridex I.V. with a concentration of 1.12 μg iron/μL.

III. RESULTS

To demonstrate the MM-ODT approach, we recorded M-mode OCT/ODT images of a glass capillary tube filled with a stationary low-susceptibility turbid solution without and with an external magnetic field as a control sample. The low-susceptibility turbid solution was a mixture of deionized water and 0.5-μm latex microspheres (scattering coefficient (μ_s)=5 mm^{-1}). The magnetic flux density and its frequency were approximately 1 T and 50 Hz, respectively. The field gradient, $\partial B/\partial z$, over 1 mm was 220 T/m. M-mode OCT/ODT images were acquired for 100 ms per frame. Figs. 3 (a) and (b) show M-mode OCT and ODT images without any external magnetic field. The ODT image (Fig. 3 (b)) contains small random phase fluctuations due to ambient vibration through the optical path. Figs. 3 (c) and (d) show M-mode OCT/ODT images with a 50 Hz externally applied magnetic field. No distinguishable Doppler shift could be observed in the ODT image (Fig. 3 (d)) indicating no interaction between the external magnetic field and the moving latex microspheres.

To simulate flow, the SPIO nanoparticle solution was injected through the glass capillary tube by a syringe pump at a constant flow rate. As Fig. 4 shows, the oscillating Doppler frequency shift resulting from nanoparticle movement could be observed at three different flow rates (3, 12, and 30 mm/s). The angle between the probing beam and the tube was set at 5% so that the wrapped Doppler frequency shift, at the high flow rate (30 mm/s), was minimized to occur only one time. "Wrapped" means that the shift moves beyond the maximum detectable range without any phase-unwrapping procedure. The probing beam was first aligned at the center of the field generating core, and the tube was placed on top of the tip so that one

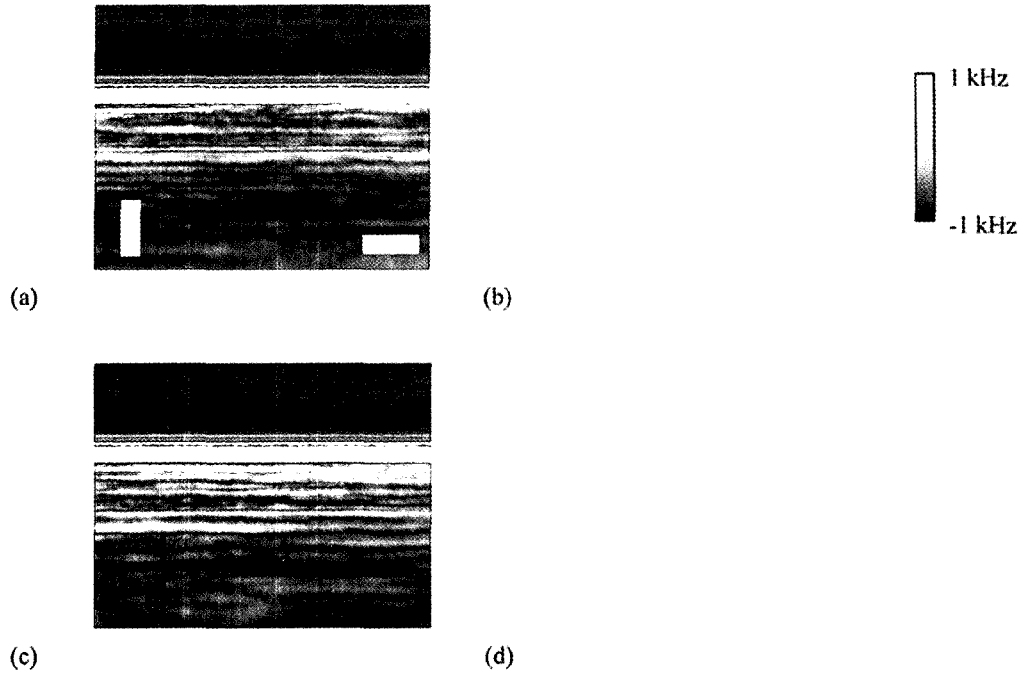

FIG. 3. OCT/ODT M-Mode images of a stationary low-susceptibility turbid solution without and with an external magnetic field. (a), (b) OCT and ODT M-Mode images without an external magnetic field, respectively. (c), (d) OCT and ODT images with a 50 Hz magnetic field, respectively. White vertical bar: 200 μm; White horizontal Bar: 20 msec.

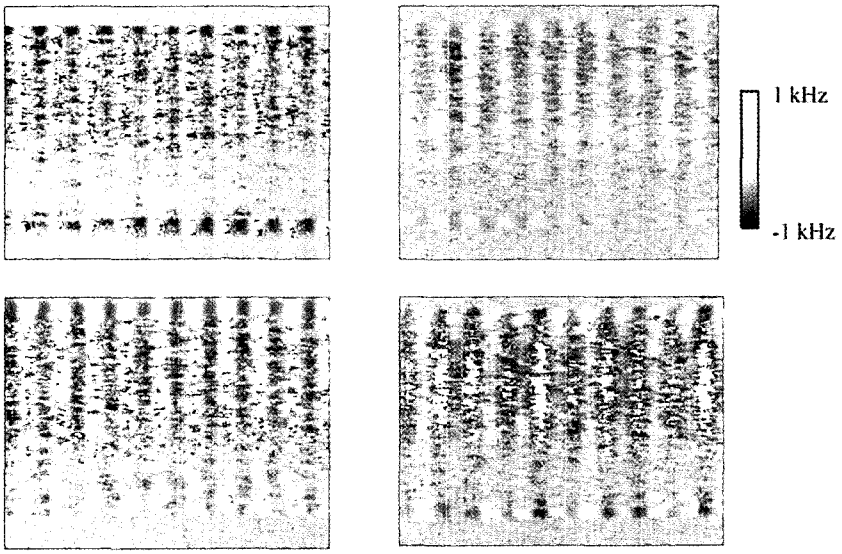

FIG. 4. M-mode MM-ODT images of diluted SPIO nanoparticle flow (1.12 μg/μL) with an externally applied 50 Hz magnetic field. (a), (b), (c), and (d): 0, 3, 12, 30 mm/s, respectively. Black vertical bar: 200 μm, Black horizontal Bar: 20 ms

can assume that the direction of the field gradient was parallel to the probing beam. M-mode MM-ODT images (Fig. 4) consisted of 634×400 pixels axially and temporally, respectively, resulting in an image acquisition time of 100 ms. The images were recorded after 5 seconds following the activation of the magnetic field.

A Doppler frequency shift of 100 Hz oscillation could be continuously observed during the magnetic activation. The oscillation frequency (100 Hz) was double that of the applied B- field (50 Hz) according to Eq. (1). The cylinder in Fig. 4, 5 a) represents the inner wall of the tube, and the arrow indicates flow direction. The vertical and horizontal bars indicate axially 200 μm and temporally 20 ms, respectively.

IV. Discussion

Superparamagnetic nanoparticles under the influence of a strong magnetic field gradient tend to travel toward the field source. As the local concentration of nanoparticles increases in response to an external magnetic field, osmotic and elastic recoil forces from the inner tube boundary increase and hinder further movement into the field. Equivalently, forces driving nanoparticles find an equilibrium state where the magnetic force is balanced by the sum of the recoil forces. When only a magnetic force is present (recoil and pressure gradient forces are absent or neglected), direct integration of Eq. (3) gives, $z(t) = \varepsilon(t) + z_o \cos(4\pi f_m t))$, where, $\varepsilon(t) = a_o t^2$ and a_o, z_o are constants and dependent on χ, V, B, and f_m is the modulation frequency of the magnetic flux density. The initial transient response of the nanoparticles to the magnetic field contains both components of *z(t)*. The SPIO nanoparticles moved in one direction and soon movement was reduced. However, the Doppler frequency oscillation could be observed at the beginning of the magnetic field. In confined systems such as a glass capillary tube or blood vessel, $\varepsilon(t)$ becomes negligible at sufficiently long times (several seconds) because recoil and drag forces impede the free-space acceleration of the nanoparticles. Like a spring response, these repelling forces eventually prohibit further the initial movement. Once these forces are equal, free-space acceleration of the SPIO nanoparticles approaches zero and the sinusoidal variation of the magnetic force dominates nanoparticle displacement.

The nanoparticles used herein are nanoscale while the probing beam had a wavelength of 1.3 μm so that individualized imaging is not possible. However, the images reported in this paper represent their aggregated response and the movement. While it has been reported that the introduction of a magnetic field changes the amplitude of the fringe [16], we applied the magnetic field in the same direction as the probing beam, so that phase changes of the nanoparticles, rather than the amplitude change, were produced and monitored. The minimum detectable concentration of nanoparticles was 0.36 μg iron/μL which is three times higher than the manufacturer recommended dilution level (0.11 μg iron/μL) for human procedures.

V. CONCLUSION

In conclusion, we have demonstrated the implementation of MM-ODT for superparamagnetic iron oxide nanoparticle imaging using an external oscillating magnetic field. Phase modulation of the nanoparticles during flow was introduced by applying a temporally oscillating high-strength magnetic field in the same direction as the probing beam. The phase change of the nanoparticles was detected in M-mode Doppler frequency imaging. The controlled and increased Doppler frequency shift in MM-ODT with superparamagnetic nanoparticles may provide a new investigational tool to identify small blood vessels and to study superparamagnetic nanoparticles dynamics for various cancer diagnostics.

*Corresponding author : jhoh@mail.utexas.edu.

REFERENCES

[1] A. F. Fercher, W. Drexler, C. K. Hitzenberger, and T. Lasser, "Optical coherence tomography - principles and applications," *Rep. Pro. Phys.*, vol. 66, pp. 239-303, 2003.

[2] B. H. Park, M. C. Pierce, B. Cense, and J. F. de Boer, "Real-time multi-functional optical coherence tomography," *Opt. Express*, vol. 11, pp. 782-793, 2003.

[3] N. J. Kemp, J. Park, H. N. Zaatari, H. G. Rylander, and T. E. Milner, "High-sensitivity determination of birefringence in turbid media with enhanced polarization-sensitive optical coherence tomography," *J. Opt. Soc. Amer. A*, vol. 22, pp. 552-560, 2005.

[4] D. P. Dave, T. Akkin, and T. E. Milner, "Polarization-maintaining fiber-based optical low-coherence reflectometer for characterization and ranging of birefringence," *Opt. Lett.*, vol. 28, pp. 1775-1777, 2003.

[5] C. G. Rylander, D. P. Dave, T. Akkin, T. E. Milner, K. R. Diller, and A. J. Welch, "Quantitative phase-contrast imaging of cells with phase-sensitive optical coherence microscopy," *Opt. Lett.*, vol. 29, pp. 1509-1511, 2004.

[6] J. F. de Boer, T. E. Milner, M. G. Ducros, S. M. Srinivas, and J. S. Nelson, "Polarization-sensitive optical coherence tomography," in *Handbook Of Optical Coherence Tomography.*, B. E. Bouma, and G. J. Tearney, eds. (Marcel Dekker, Inc, New York, 2002), pp. 237-274.

[7] Z. P. Chen, T. E. Milner, D. Dave, and J. S. Nelson, "Optical Doppler tomographic imaging of fluid flow velocity in highly scattering media," *Opt. Lett.*, vol. 22, pp. 64-66, 1997.

[8] X. J. Wang, T. E. Milner, and J. S. Nelson, "Characterization of Fluid-Flow Velocity by Optical Doppler Tomography," *Opt. Lett.*, vol. 20, pp. 1337-1339, 1995.

[9] Y. H. Zhao, Z. P. Chen, C. Saxer, S. H. Xiang, J. F. de Boer, and J. S. Nelson, "Phase-resolved optical coherence tomography and optical Doppler tomography for imaging blood flow in human skin with fast scanning speed and high velocity sensitivity," *Opt. Lett.*, vol. 25, pp. 114-116, 2000.

[10] B. H. Park, M. C. Pierce, B. Cense, S. H. Yun, M. Mujat, G. J. Tearney, B. E. Bouma, and J. F. de Boer, "Real-time fiber-based multi-functional spectral-domain optical coherence tomography at 1.3 um," *Opt. Express*, vol. 13, pp. 3931-3944, 2005.

[11] M. C. Pierce, B. H. Park, B. Cense, and J. F. de Boer, "Simultaneous intensity, birefringence, and flow mea-

surements with high-speed fiber-based optical coherence tomography," *Opt. Lett.*, vol. 27, 1534-1536, 2002.

[12] D. Q. Piao, and Q. Zhu, "Quantifying Doppler angle and mapping flow velocity by a combination of Doppler-shift and Doppler-bandwidth measurements in optical Doppler tomography," *Appl. Opt.*, vol. 42, pp. 5158-5166, 2003.

[13] T. M. Lee, A. L. Oldenburg, S. Sitafalwalla, D. L. Marks, W. Luo, F. J. J. Toublan, K. S. Suslick, and S. A. Boppart, "Engineered microsphere contrast agents for optical coherence tomography," *Opt. Lett.*, vol. 28, pp. 1546-1548, 2003.

[14] C. Loo, A. Lin, L. Hirsch, M. H. Lee, J. Barton, N. Halas, J. West, and R. Drezek, "Nanoshell-enabled photonics-based imaging and therapy of cancer," *Technol. Cancer Res. Treat.*, vol. 3, pp. 33-40, 2004.

[15] A. L. Oldenburg, J. R. Gunther, and S. A. Boppart, "Imaging magnetically labeled cells with magnetomotive optical coherence tomography," *Opt. Lett.*, vol. 30, pp. 747-749, 2005.

[16] A. L. Oldenburg, F. J. J. Toublan, K. S. Suslick, A. Wei, and S. A. Boppart, "Magnetomotive contrast for in vivo optical coherence tomography," *Opt. Express*, vol. 13, pp. 6597-6614, 2005.

[17] Y. X. J. Wang, S. M. Hussain, and G. P. Krestin, "Superparamagnetic iron oxide contrast agents: physicochemical characteristics and applications in MR imaging," *Eur. Radio.*, vol. 11, pp. 2319-2331, 2001.

[18] A. K. Fahlvik, J. Klaveness, and D. D. Stark, "Iron-Oxides as Mr Imaging Contrast Agents," *J. Magn. Reson. Imaging.*, vol. 3, pp. 187-194, 1993.

[19] R. Weissleder, A. Bogdanov, E. A. Neuwelt, and M. Papisov, "Long-Circulating Iron-Oxides for Mr-Imaging," *Adv. Drug Deliv. Rev.*, vol. 16, pp. 321-334, 1995.